

# Quantitative analysis of current density distributions from magneto-optical images of superconducting $\text{YBa}_2\text{Cu}_3\text{O}_{7-\delta}$ thin films

I B Rutel<sup>1,2</sup>, C McIntosh<sup>1,2</sup>, A Caruso<sup>1,2</sup>, M W Davidson<sup>1,2</sup> and J Schwartz<sup>1,2</sup>

<sup>1</sup> National High Magnetic Field Laboratory, Florida State University, 1800 E Paul Dirac Dr, Tallahassee, FL 32310, USA

<sup>2</sup> Department of Mechanical Engineering, FAMU-FSU College of Engineering, Tallahassee, FL 32310, USA

E-mail: rutel@magnet.fsu.edu

Received 17 November 2003

Published 30 March 2004

Online at [stacks.iop.org/SUST/17/S269](http://stacks.iop.org/SUST/17/S269) (DOI: 10.1088/0953-2048/17/5/034)

## Abstract

The magneto-optical imaging technique is applied to  $\text{YBa}_2\text{Cu}_3\text{O}_{7-\delta}$  (YBCO) thin film coated conductors, providing a visual investigation of sub-millimetre aberrations and fracture defects. The further application of post-processing techniques provides a quantitative analysis of varying patterns resulting from field penetration in the YBCO coated conductor investigations. Application of theory provides critical current information for geometries where the conduction path is perpendicular to the applied field in micro-bridge samples. A Maxwell curl calculation is performed on the intensity distribution of various images. These calculations reveal boundaries for current paths via relative screening current determination and striations.

## 1. Introduction

Magneto-optical imaging (MOI) is a useful tool for imaging the magnetic field associated properties of various materials [1, 2]. MOI has been applied to superconducting samples in small fields, providing visual information about the magnetic flux distribution, flux dynamics in bulk conductors [3, 4], flux penetration into irradiated conductors [5], and flux penetration within filaments of powder in tube conductors [6] and along networks of grain boundaries in thin film superconducting tapes, deposited on crystalline substrates with various composite layers (coated conductors) [7–17]. The MOI technique has also been employed to experimentally determine current densities of various conductors by determining a field distribution from a current density theory (Biot–Savart) or from an inverted Biot–Savart calculation to determine the current densities directly [18, 19]. The focus of these calculations is to determine a calibrated value for the current distribution and is not a trivial problem [20–24].

It is possible, however, to obtain useful information about the sample by determining a relative current distribution. Indiscernible surface characteristics which may have previously not been noticed may be found without intensive calculations. By employing a relatively simple algorithm and calculating a component of the current density ( $\vec{j}(x, y)$ ) via the curl of the field penetration (Maxwell's equation),

$$\vec{\nabla} \times \vec{B} = \mu_0 \vec{J}, \quad (1)$$

information about the onset of cracking from applied strain, and colony boundaries/current paths may be seen.

$\text{YBa}_2\text{Cu}_3\text{O}_{7-\delta}$  (YBCO) has one of the largest current carrying capacities of the high temperature superconductors, and has seen recent advancements with production technology that indicate substantial technological potential [25, 26]. With production improvements comes the need for better evaluation techniques to determine the influence of production and application of stress on the conductor magnetic behaviour.

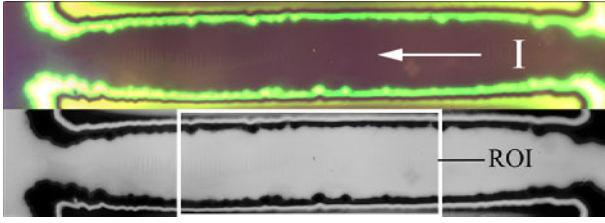


**Figure 1.** Top: image of the raw image converted to greyscale. The arrow indicates the current flow direction. Bottom: inverted greyscale image with suggested region of interest (ROI).

(This figure is in colour only in the electronic version)

We focus on samples in the remnant state, where a field has been applied and then removed, trapping flux in the penetrated portions of the YBCO coated conductor.

Emphasis on the MOI technique is usually placed on the raw images acquired from field penetration. This technique is, in general, useful and relatively easy to analyse. However, it may be prudent to investigate the information one can gain by introducing more sophisticated analysis methods.

## 2. Experimental details

The experiment is carried out in a flow through cryostat which reaches temperatures of  $\sim 30$  K. The samples are placed on a copper platform connected to the heat transfer point via a sapphire cylinder. Samples are then zero-field cooled (ZFC) and subjected to a field of up to 100 mT from an external magnet. The MOI film is placed on top of the samples and images are then taken through the polarizer/dark field microscope configuration. The images are then stitched together and analysed using the methods described below.

We present two different methods, developed using the Labview software programming environment. This particular environment is convenient due to the many image handling functions already available. The environment includes a simple interface for inserting raw code, allowing for analysis variations not included with commercial software. The analysis program described here analyses TIFF images with sizes of  $\sim (12\,000 \times 2000)$  pixels.

The first analysis determines the critical current density ( $j_c$ ) from an annihilation theory developed by Baziljevich *et al* [27] for superconducting films with a perpendicular applied magnetic field. A bridge of superconducting film, when placed in the remnant state by a field applied perpendicular to the surface, retains trapped flux. The amount of flux is determined by the sample temperature, magnitude of the applied field, and the critical current of the bridge. The trapped flux will also interact with an induced anti-flux, creating annihilation zones, areas where the net field is zero. The Baziljevich model is based on work done by Brandt *et al* where a perpendicular magnetic field is applied to a type-II superconducting strip [28]. This model accounts for several issues not addressed by Bean's critical state model [29], including the demagnetization effects consistent with the perpendicular geometry (as opposed to Bean's parallel configuration with negligible demagnetizing effects), screening currents which shield the interior of the sample (where in the Bean model areas without field

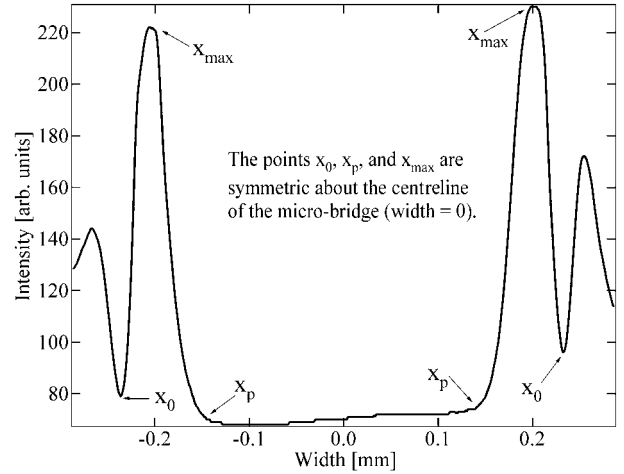


**Figure 2.** Intensity profile determined from the average of pixel values in the ROI along the current direction.  $x_p$ ,  $x_0$  and  $x_{max}$  are the maximum field penetration, centre of the annihilation zone and maximum field value, respectively.

penetration have no screening currents), and rectangular (instead of ellipsoidal) cross sections [28–30].

The annihilation zones, when imaged by MOI, remain dark. Dark areas, however, are not exclusively annihilation zones; areas that are not superconducting at the local field and temperature will also be dark due to the absence of trapped flux. This pattern is seen as the alternating bands of dark and light in the upper image of figure 1. The lower image has been converted to a greyscale mode and inverted from the actual picture to set the pixel value within the annihilation zones to a greyscale value of zero. A region of interest (ROI) can then be defined, which is best limited to the area closest to the centre of the bridge, in order to reduce edge influences. The ROI is averaged over the length of the conductor along the current direction, helping to remove random effects contributed from synthesis factors. The averaged profile (figure 2) is then analysed by employing the Baziljevich method.

First, three points are extracted from the profile plot in figure 2.  $x_p$ ,  $x_0$  and  $x_{max}$  are the maximum field penetration, centre of the annihilation zone and maximum field value, respectively, and are determined using the distance between each of their respective points on either side of the centreline of the film width ( $2a$ ) and halved. These values are then input into the following equations from [27] resulting in a value for the critical current density ( $j_c$ ) and maximum penetration field ( $B_{max}$ ):

$$j_c(x) = \frac{\pi B_a^{\max}}{\mu_0 d} \left[ a \cosh \frac{1 + [1 - (x_0/a)^2] \sqrt{2 + (a/x_0)^2}}{2(x_0/a)^2 - 1} \right]^{-1} \quad (2)$$

$$B(x, B_a, j_c) = \begin{cases} 0, & |x| < x_p \\ B_c a \tanh \sqrt{(1 - (x_p/x)^2)/(1 - (x_p/a)^2)}, & x_p < |x| < a \\ B_c a \tanh \sqrt{(1 - (x_p/a)^2)/(1 - (x_p/x)^2)}, & |x| > a, \end{cases} \quad (3)$$

where in equation (2)  $B_a^{\max}$  is the maximum applied field,  $d$  is the thickness of the conductor,  $\mu_0$  is the permeability of free space, and in equation (4)  $B_c = \mu_0 j_c d / \pi$  is defined as the critical field.

This method is a useful, non-destructive calculation for the  $j_c$  of the conductor. Since the calculation is done over an averaged portion of the sample, the values can be considered a thermodynamic bulk measurement of the magnetization (trapped flux). Thus, the technique also allows for various cracks, boundaries and other current impediments to be present without adding large error to  $j_c$ .

The second calculation is a relatively simple application of Maxwell's curl equation of  $\vec{B}$  to determine a component of  $\vec{j}(x, y)$ . A program was designed to employ the discrete differentiation of directional derivatives determined from equation (1).

The assembled image (figure 1) is converted to an inverted greyscale image and then from a TIFF format ( $12\,000 \times 2\,000$  pixels) to an array of pixels ( $12\,000 \times 2\,000$  points). Each of the points in the array takes the corresponding greyscale value (0–255) from the image. The discrete differentiation is then applied to the array with care taken in determining the values in both the  $x$  and  $y$  directions, resulting in the partial derivatives  $\partial B_z / \partial y$  and  $\partial B_z / \partial x$ . The terms are then added in quadrature to determine the magnitude of the resultant component of  $\vec{j}(x, y)$ , dependent on the  $z$  component of the remnant magnetic field trapped in the conductor. The array is then scaled to the greyscale range (0–255), and returned to a JPEG image format.

During the process of calculating the curl component, we also determine statistical measures of the current density distribution. We find the average and standard deviation of the intensity along both the  $x$  and  $y$  directions. These indicators provide a quantitative means of interpreting the curl calculation data. Finding large standard deviations indicates areas with widely varying values compared to the background and suggests areas of large screening currents. These areas may be colony boundaries, voids, fracture nucleations, or MOI indicator film defects.

### 3. Results/discussion

We apply the first method to a YBCO micro-bridge on a single crystal substrate. This sample is shown in figure 1 and the corresponding profile average seen in figure 2 for a temperature of 25 K and 50 mT of applied field. The result of the  $j_c$  calculation is seen in figure 3 for varying temperatures and applied fields. The sample can then be analysed by fitting this data to an SNS type junction theory [27, 31, 32]. The SNS theory is employed due to the reasonable fit it gives to our data, which is indicative of the weak intragranular coupling of our samples (well known in YBCO conductors), matching our data to similar behaviour found in flux creep models [33]. The data is fit to the exponential equation

$$j_c = j_{c0} \exp(-A\sqrt{T/T_c}). \quad (4)$$

Using this fit we find for this sample a value of  $j_{c0} = 379.5 \text{ MA cm}^{-2}$  and a  $j_c(77 \text{ K}) = 19.2 \text{ MA cm}^{-2}$ . The presented values should then be an upper limit on the values

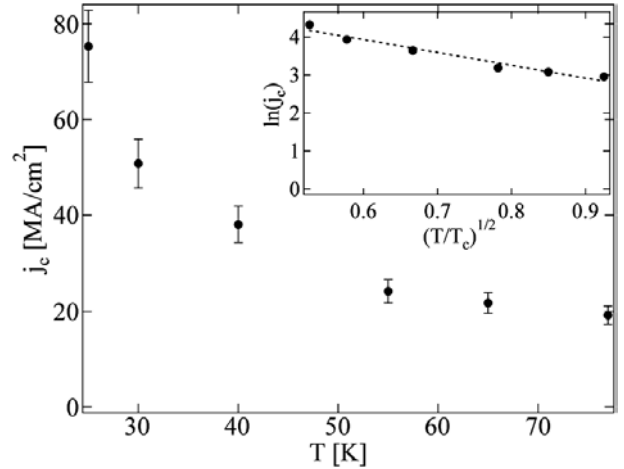


**Figure 3.** Plot of the calculated critical current density calculations using the Baziljevich method [27]. Inset: fit of exponential to data showing good agreement with the SNS flux creep model [33].

of the critical current density through the micro-bridge. The  $j_c(77 \text{ K})$  value is corroborated with a transport measurement on the sample, by the crystal growers, and is measured to be  $8.3 \text{ MA cm}^{-2}$ . The value predicted by the MOI method is larger than that of the transport experiment, which is suggestive of the bulk nature of the MOI method and is not affected by interruptions in the current path. The annihilation analysis is limited to a fairly small number of geometric situations, where in the above case a reasonable estimation can be determined for our samples of micro-bridges with rectangular geometry. Further development is required to apply this method to more complex situations (i.e. self-field transport, transverse field, etc).

The second method, where we calculate the curl of the remnant field, does not provide the quantitative values of critical current, but does provide a robust method of enhancing the detail of the MOI images. When we apply the curl method to this sample we get the result shown in figure 4(a). We can also apply it to various coated conductor samples, one of which is shown in figure 4(b). In both of these samples the colonies are indicated by the darker areas inside the boundary of the white outlines. The white areas indicate large curl values (and hence large screening currents), and the darker areas retain no trapped current (either superconducting colonies which were not penetrated by the applied flux or non-superconducting regions). Also note in figure 4(a) the light white striations present in the sample, having a periodicity of  $\sim 90 \mu\text{m}$ ; such detail was not apparent in the raw imaging. The potential to visualize features not shown in the raw images may lead to investigations on requirements for minimal crack nucleation and growth from the induced strain [34].

Figure 5 shows a micro-bridge sample which has some structure (either a grain boundary or a fracture line). Note the large screening current surrounding the structural defect. Although noticeable in the magnetic field distribution in this image, one may consider structural defects which are much smaller, and may not be as apparent in the raw image. These types of defect may then be enhanced by mapping the local relative change in the calculated component of  $\vec{j}(x, y)$ . The analysis provides a resolution of features to about  $1 \mu\text{m}$  which

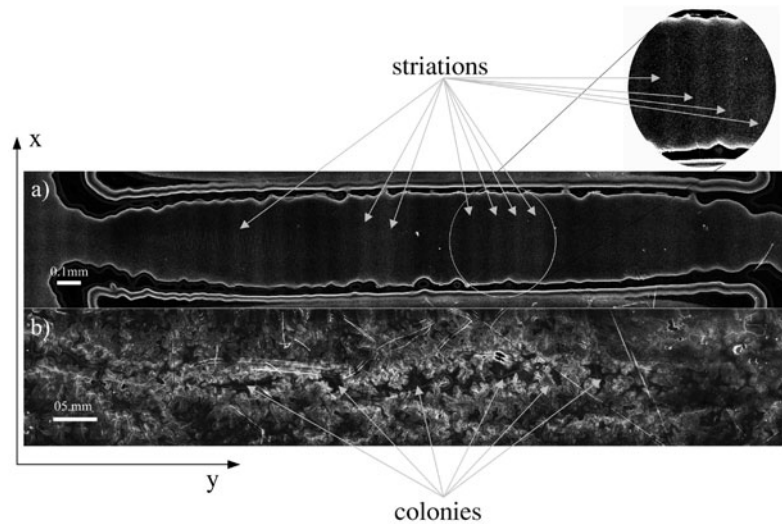


**Figure 4.** (a) The current density distribution for a micro-bridge sample. Note the striations that appear about every  $90 \mu\text{m}$ . (b) The current density distribution for a YBCO coated conductor. Note the central dark region outlined by bright outlines, this is the colony boundary of the superconducting region.

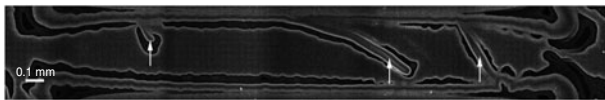


**Figure 5.** Current density distribution for micro-bridge with defects. Bright areas indicated by arrows show the screening currents from superconducting regions around the defect edges, outlining aberrations in the conduction path.

is about  $3\times$  the thickness of the sample ( $0.3 \mu\text{m}$ ). We can utilize this resolution to investigate features of inclusions on this length scale, colony details and microstructural crack propagation.

Our final method of adding quantitative data to the qualitative MOI imaging technique is to apply statistical averaging. We use a simple average and standard deviation calculation to form profiles of the images along both directions for the calculated component of  $\vec{j}(x, y)$ . Presented in figure 6, we show a statistical profile for both the micro-bridge sample and the coated conductor sample. When investigating these plots, the periodic areas of higher intensity are clearly shown in the  $x$  direction for the micro-bridge sample. Also the homogeneity of the coated conductor can be sampled by observing regions of low standard deviation (along the  $y$  direction) in the centre of the conductor, where there are regions of large colony growth in the rolling direction of the sample. Both plots add quantitative information, enhancing the information collected from the raw MOI images.

#### 4. Conclusion

We present two methods for interpreting MOI images via analytical post-processing. The first method applies theory from a perpendicular applied magnetic field to ascertain  $j_c$  non-destructively. At present this analysis is presented only for this particular geometry, however it is possible to expand this technique to other conductor geometries as well as including transport current. The second method determines

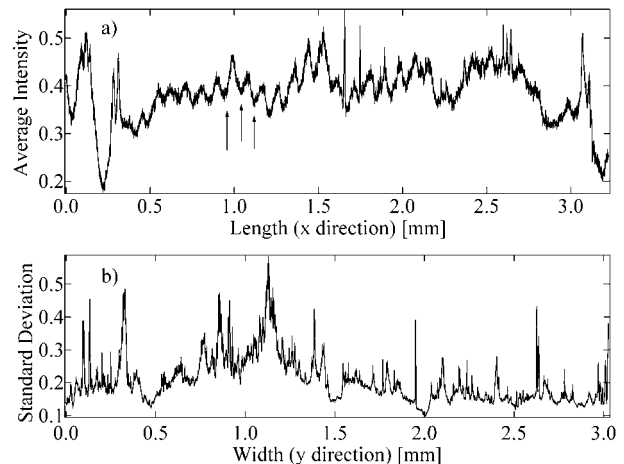


**Figure 6.** (a) The statistical average of the intensity for the calculated component of  $\vec{j}(x, y)$  along the  $x$  direction for the micro-bridge sample. Arrows indicate the varying periodic intensity seen in the current density plot, and are  $\sim 90 \mu\text{m}$  apart. (b) The statistical standard deviation calculated for the calculated component of  $\vec{j}(x, y)$  along the  $y$  direction for the coated conductor sample. Note the low standard deviation values at 1.5 and 2 mm, which are towards the centre of the image and outline the dark areas, regions of screened superconductor colonies.

a component of the relative  $\vec{j}(x, y)$  distributions, conductor inhomogeneities, and can show the magnetic microstructure. The method is a simple application of Maxwell's equation but provides a powerful method to employ in such instances as the quality control of conductor production. In combination with introducing a statistical calculation, the described methods add a quantitative assessment to the qualitative technique of MOI.

#### Acknowledgments

We thank R Nekkanti and P Barnes at the AFRL/PRPG for samples, and acknowledge support from the AFOSR.

## References

- [1] Larbalestier D, Gurevich A, Feldmann D M and Polyanskii A 2001 *Nature* **414** 368
- [2] Welp U, Berger A, Miller D J, Vlasko-Vlasov V K, Gray K E and Mitchell J F 1999 *Phys. Rev. Lett.* **83** 4180
- [3] Turchinskaya M, Kaiser D L, Gayle F W, Shapiro A J, Roytburd A, Vlasko-Vlasov V, Polyanskii A and Nikitenko V 1993 *Physica C* **216** 205
- [4] Durán C A, Gammel P L, Wolfe R, Fratello V J, Bishop D J, Kimura T, Kitazawa K and Kishio K 1994 *Phys. Rev. B* **49** 3608
- [5] Turchinskaya M, Kaiser D L, Shapiro A J and Schwartz J 1993 *Physica C* **246** 375
- [6] Liu H K, Polyanskii A, Chen W M, Guo Y C, Dou S X and Apperley M 2001 *IEEE Trans. Appl. Supercond.* **11** 3764
- [7] Batalla E, Zwart E G, Goudreaux R and Wright L S 1990 *Rev. Sci. Instrum.* **61** 2194
- [8] Welp U, Gunter D O, Crabtree G W, Zhong W, Balachandran U, Haldar P, Sokolowski R S, Vlasko-Vlasov V K and Nikitenko V I 1995 *Nature* **376** 44
- [9] Polyanskii A A, Gurevich A, Pashitski A E, Heinig N F, Redwing R D, Nordman J E and Larbalestier D C 1996 *Phys. Rev. B* **53** 8687
- [10] Zamboni M, Yoo S I, Higuchi T, Waki K, Koishikawa S and Murakami M 1997 *Physica C* **281** 218
- [11] Feldmann D M, Reeves J L, Polyanskii A A, Kozlowski G, Biggers R R, Nekkanti R M, Maartense I, Tomsic M, Barnes P, Oberly C E, Peterson T L, Babcock S E and Larbalestier D C 2000 *Appl. Phys. Lett.* **77** 2906
- [12] Bobyl A V, Shantsev D V, Johansen T H, Baziljevich M, Galperin Y M and Gaevski M E 2000 *Supercond. Sci. Technol.* **13** 183
- [13] Das A, Muralidhar M, Koblischka M R and Murakami M 2000 *Physica C* **338** 284
- [14] Giller D, Shaulov A, Dorosinskii L, Tamegai T and Yeshurun Y 2000 *Physica C* **341** 1089
- [15] Feldmann D M, Reeves J L, Polyanskii A A, Goyal A, Feenstra R, Lee D F, Paranthaman M, Kroeger D M, Christen D K, Babcock S E and Larbalestier D C 2001 *IEEE Trans. Appl. Supercond.* **11** 3772
- [16] Reeves J L, Feldmann D M, Yang C Y and Larbalestier D C 2001 *IEEE Trans. Appl. Supercond.* **11** 3863
- [17] Giller D, Kalisky B, Shaulov A, Tamegai T and Yeshurun Y 2001 *J. Appl. Phys.* **89** 7481
- [18] Polyanskii A A, Gurevich A, Pashitski A E, Heinig N F, Redwing R D, Nordman J E and Larbalestier D C 1995 *Phys. Rev. B* **53** 8687
- [19] Johansen T H, Baziljevich M, Bratsberg H, Galperin Y, Lindelof P E, Shen Y and Vase P 1996 *Phys. Rev. B* **54** 16264
- [20] Niculescu H, Saenz A, Khankhasayev M and Gielisse P J 1996 *Physica C* **261** 12
- [21] Brandt E H 1995 *Phys. Rev. Lett.* **74** 3025
- [22] Brandt E H 1995 *Phys. Rev. B* **52** 15442
- [23] Wijngaarden R J, Spoelder H J W, Surdeanu R and Griessen R 1996 *Phys. Rev. B* **54** 6742
- [24] Jooss Ch, Warthmann R, Forkl A and Kronmüller H 1997 *Physica C* **299** 215
- [25] Goyal A, List F A, Mathis J, Paranthaman M, Specht E D, Norton D P, Park C, Lee D F, Kroeger D M, Christen D K, Budai J D and Martin P M 1998 *J. Supercond.* **11** 481
- [26] Goyal A *et al* 2001 *Physica C* **357** 903
- [27] Baziljevich M, Johansen T H, Bratsberg H, Galperin Y, Lindelof P E, Shen Y and Vase P 1996 *Physica C* **266** 127
- [28] Brandt E H and Indenbom M 1993 *Phys. Rev. B* **48** 12893
- [29] Bean C P 1962 *Phys. Rev. Lett.* **8** 250
- [30] Ravi Kumar G and Chaddah P 1988 *Phys. Rev. B* **39** 4704
- [31] Kadowaki K, Songliu Y and Kitazawa K 1994 *Supercond. Sci. Technol.* **7** 519
- [32] De Vries J W C, Stollman G M and Gijs M A M 1989 *Physica C* **157** 406
- [33] Mannhart J, Chaudhari P, Dimos D, Tsuei C C and McGuire T R 1988 *Phys. Rev. Lett.* **61** 2476
- [34] van der Laan D C, van Eck H J N, Davidson M W, ten Haken B, ten Kate H H J and Schwartz J 2002 *Physica C* **372–376** 1020